Available online at www.sciencedirect.com
ScienceDirect
Journal of Power Sources 172 (2007) 553–559
JOURNAL OF POWER SOURCES
www.elsevier.com/locate/jpowsour

Reduction of carbon dioxide gas formation at the anode of a direct methanol fuel cell using chemically enhanced solubility

Michael D. Lundin, Mark J. McCready *

181 Fitzpatrick Hall, Department of Chemical & Biomolecular Engineering, University of Notre Dame, Notre Dame, IN 46556, United States

Received 20 April 2007; received in revised form 15 May 2007; accepted 17 May 2007
Available online 25 May 2007

Abstract

The production of CO_2 gas at the DMFC anode leads to dramatic increases in pumping power requirements and reduced power output because of mass transfer limitations as bubble trains form in the channels of larger stacks. Experimental observations taken in a 5 cm^2 DMFC test cell operated at 60 °C, 1 atm, and with a methanol/water fuel flow rates of 5–10 $cm^3\,min^{-1}$ indicate that the rate of bubble formation can be reduced by increasing the fuel flow because more liquid is available for the CO_2 to dissolve in. Further observations indicate that KOH and LiOH added to the fuel eliminates CO_2 gas formation in situ at low concentrations because of the greatly increased solubility that results.

A mathematical model for the volumetric rate of CO_2 gas production that includes effects of temperature and solubility is developed and extended to include the effects of hydroxide ions in solution. The model is used to predict the onset location of gas formation in the flow field as well as the void fraction at any point in the flow field. Predictions from the model agree very well with our experiments. Model predictions explain differences in the initial location of bubble formation for fuel solutions pre-saturated with CO_2 as opposed to CO_2-free solutions. Experiments with KOH and LiOH added to fuel solutions confirm the validity of the model extension that includes solubility that is enhanced by chemical reaction.

Experiments with LiOH, KOH, and ammonium hydroxide show that the long-term durability of standard Pt–Ru/Nafion®/Pt membrane electrode assemblies is compromised because of the presence of lithium, potassium, and ammonium cations that interact with the Nafion® membrane and result in increasing the ohmic limitations of the polymer electrolyte membrane. Experiments with $Ca(OH)_2$, while reducing gas formation, precipitate the product $CaCO_3$ out of solution too rapidly for downstream filtering, blocking channels in the flow field.

Keywords: DMFC; CO_2 bubbles; Two-phase flow; Gas reduction

1. Introduction

Since its conception, the fuel cell has been attractive for the conversion of chemical energy into electrical energy due to high efficiencies and low emissions. While H_2 powered cells have numerous potential applications, the need to power portable devices is driving development of fuel cells with liquid fuels.

Liquid methanol has a higher energy density than hydrogen and other gas fuels and is more easily processed and stored. The direct methanol fuel cell (DMFC) takes advantage of these properties and is a potential power source for portable applications; however, its current shortcomings in kinetics and methanol crossover problems yield a power density nearly an order of magnitude lower than that of a hydrogen fueled PEMFC [1]. Because of those limitations, every opportunity to optimize cell operation must be considered.

The DMFC consists of a polymer electrolyte membrane with anode and cathode catalyst layers on either side. Gas diffusion layers made of either carbon paper or carbon cloth are used to cover the catalyst layers to enhance diffusion and create electrical contact between the catalyst layers and current collectors on each end. The current collectors have some machined flow channel pattern in the surface that allows supply of fuel and oxidants. In a DMFC methanol is oxidized in the presence of water to CO_2 at the anode while oxygen is reduced to water at the cathode. Operating temperatures are generally held below 100 °C to prevent boiling of the fuel. The following reactions describe the process:

$$\text{Anode reaction}: \quad CH_3OH + H_2O \rightarrow CO_2 + 6H^+ + 6e^-; \tag{1}$$

* Corresponding author. Tel.: +1 574 631 7146; fax: +1 574 631 8366.
E-mail address: mjm@nd.edu (M.J. McCready).

0378-7753/$ – see front matter © 2007 Elsevier B.V. All rights reserved.
doi:10.1016/j.jpowsour.2007.05.074

$$\text{Cathode reaction}: \quad (3/2)O_2 + 6H^+ + 6e^- \rightarrow 3H_2O; \qquad (2)$$

$$\text{Overall reaction}: \quad CH_3OH + (3/2)O_2 \rightarrow CO_2 + 2H_2O. \qquad (3)$$

To ensure maximum current density and optimal reaction conditions, efficient removal of both CO_2 from the anode surface and water from the cathode surface is essential. While water management at the cathode has been studied [2] due to its occurrence in H_2 PEM cells, removal of CO_2 at the anode has been largely overlooked and remains an important issue for research in the development of DMFCs.

In the typical DMFC, methanol in a low concentration (1 M) solution is fed to the anode flow field and contacts the anode catalyst via the diffusion layer while the CO_2 being produced traverses the diffusion layer to the anode flow field in reverse. The quantity of CO_2 being produced is directly related to current produced by the cell. Combining Faraday's constant with the anode stoichiometry from (1), CO_2 in the amount of 1.036×10^{-4} mol min^{-1} Amp^{-1} is produced. The fuel for the reaction is liquid water and methanol, so the CO_2 produced at the anode is initially in the liquid phase. Because of the large quantities of CO_2 that evolve, the liquid fuel quickly becomes saturated and gas phase CO_2 forms. This gas formation, under poorly optimized operating conditions, may consume a significant fraction of the flow field volume. CO_2 gas limits mass transfer of methanol and water to the anode catalyst surface and the presence of gas is indicative that the fuel solution is saturated with CO_2 and that diffusion of CO_2 from the catalyst surface may be limited. Initiation of two-phase flow leads to a capillary bubble train in the flow field creating pressure drops that decrease the efficiency of a stack by both increasing pumping power requirements and methanol crossover. In portable systems the problem of fuel supply is generally overcome by increasing the flow rate of the anode fuel, which can have the undesirable side effects of further increasing methanol crossover and creating temperature gradients if the fuel solution is not properly pre-heated. Unfortunately, the formation of capillary bubble trains at high current production is inevitable even under these conditions.

The topic of CO_2 gas evolution in DMFCs has received some attention in the literature. Gas bubble growth and release from the diffusion layer was investigated by Mench et al. [3]. Argyropoulos et al. [4] witnessed the blocking of parallel flow channels at low flow rates and high current densities while studying the CO_2 flow characteristics visually in situ. Yang et al. [5] conducted a comprehensive investigation into effects of flow field designs and cell orientation while qualitatively studying CO_2 bubble behavior using visualization in situ. While Yang et al. did not encounter the channel blocking slugs that Argyropoulos encountered, they did show that the presence of large gas slugs in the flow field correlated to decreased cell performance.

In this paper, a model for the volume rate of CO_2 gas production is presented which depends on the operating temperature of the cell, current produced by the cell, feed rate of fuel to the anode, and the solubility of CO_2 in the fuel as a function of temperature. Extensions of this model to include additional parameters that could contribute to gas reduction are briefly discussed. Experimental results validating the original model are then presented as well as results from experiments exploring possible options for delaying the onset of gas formation. Reactants considered for gas onset delay enhancement include NaOH, LiOH, $Ca(OH)_2$, and ammonium hydroxide. The long-term durability of standard Pt–Ru/Nafion®/Pt membrane electrode assemblies (MEAs) is investigated as it relates to these reactants.

Under conditions when two-phase flow occurs, the ability to characterize it is important from a design standpoint so that problems relating to heat transfer, mass transfer, and pressure drop all may be avoided. A key property of two-phase flow characterization is the void fraction and, to this end, the model described in this paper is used to develop expressions determining exactly when gas will begin forming in the anode flow field.

2. Theoretical expression for volumetric gas formation

2.1. General expression

The anticipated quantity of gas formation in can be related to the current discharge from the cell on a molar basis by

$$\frac{dn}{dt} = \frac{i_x L}{6F}, \qquad (4)$$

which is derived from Eq. (1) with the aid of Faraday's constant, F, where n is the molar quantity of CO_2 generated, and i_x is the total output current divided by the length of the channel, L.

If the liquid fuel is not saturated with CO_2 prior to entering the cell, then there is some capacity for CO_2 to remain dissolved in the liquid after its generation at the anode surface, thus not appearing in the gas phase. For the length of cell flow path where the fuel is not saturated with CO_2, the appearance of bubbles will depend on the rate of CO_2 formation by reaction and the local fluid mixing. If the CO_2 production rate is sufficiently high and the bubbles are effectively nucleated, then CO_2 gas phase will appear even if the fuel is not saturated with CO_2. This would most likely occur at higher currents.

In the region where all of the CO_2 remains in the liquid phase, the change in concentration in the liquid can be calculated using a mass balance on a differential slice of the channel to get

$$q_{\text{fuel}} \frac{dC_{CO_2}}{dx} = \frac{i_x}{6F}, \qquad (5)$$

where q_{fuel} is the volumetric liquid flow rate, x the distance along the channel, and C_{CO_2} is the concentration of CO_2 in the liquid in mol l^{-1}. Integrating Eq. (5) gives the CO_2 concentration in the liquid as a function of distance along the flow path:

$$C_{CO_2}(x) = \frac{i_x x}{6F q_{\text{fuel}}}. \qquad (6)$$

While high methanol concentrations can impact the solubility of CO_2 in ternary systems, a 1 M concentration typically used in a DMFC, the solubility can be approximated as water [6]. For the limited conditions where a typical DMFC is operated under atmospheric pressure in the temperature range of 298–373 K, Carroll et al. [7] gives detailed Henry's law correlations for the solubility of CO_2 in water. Considering Eq. (6) and the results

of Carroll et al., the distance into the channel where the liquid becomes saturated, x_{sat}, will be

$$x_{sat} = \frac{6Fq_{feed}C^{sat}_{CO_2}(T)}{i_x}, \quad (7)$$

where $C^{sat}_{CO_2}(T)$ is the saturation concentration of the liquid fuel solution. At distances greater than x_{sat}, gas will begin to form. Using the rate of CO_2 production from Eq. (4) and the ideal gas law, the change in the volumetric gas flow rate, q_{CO_2}, with respect to distance will be

$$\frac{dq_{CO_2}}{dx} = \frac{RT}{P}\frac{i_x}{6F}, \quad (8)$$

which can be integrated to give the gas flow rate at any location in the flow field channel:

$$q_{CO_2} = \begin{cases} 0 & x \le \dfrac{6Fq_{fuel}C^{sat}_{CO_2}(T)}{i_x} \\ \dfrac{RT}{P}\dfrac{i_x}{6F}(x - x_{sat}) & x > \dfrac{6Fq_{fuel}C^{sat}_{CO_2}(T)}{i_x} \end{cases}. \quad (9)$$

Results from Eq. (9) are displayed in Fig. 1, where a temperature of 60 °C, a pressure of 1 atm, and a current of 3 Amps over the entire flow path of arbitrary length, operated with various fuel flow rates. As the flow rate of the fuel is increased, the capacity to contain CO_2 in the liquid phase gets larger, resulting in an extension in the delay of gas formation.

2.2. Void fraction

Because void fraction is a useful characterization of two-phase flow, taking Eq. (9) one step further results in

$$\phi = \text{gas fraction} = \left[\frac{q_{CO_2}}{q_{fuel} + q_{CO_2}}\right], \quad (10)$$

which assumes that a negligible amount of liquid is consumed by the reaction. Fig. 2 displays the sudden rise in void fraction after the initial onset of gas formation and is generated using the operating parameters of 60 °C, 1 atm, 3 Amps, a flow field of arbitrary length, and various fuel feed rates. Under these conditions, small cells which should only require small amounts of fuel require high fuel flow rates simply to keep the void fraction in check.

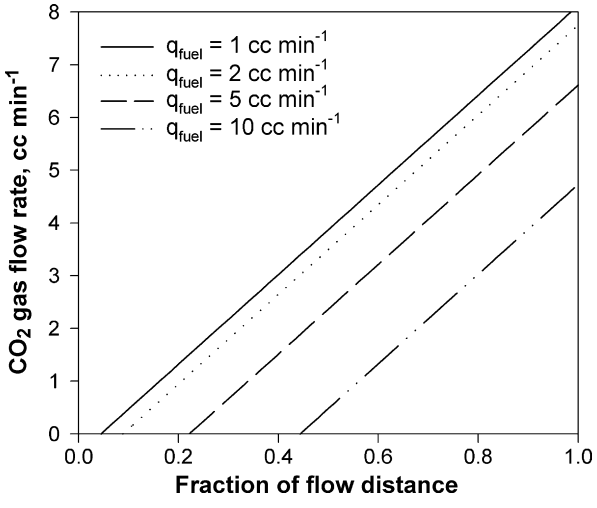

Fig. 1. The gas flow rate predicted by Eq. (9) is displayed for a variety of fuel flow rates with respect to the fraction of the flow distance (T = 60 °C, P = 1 atm, i = 3 Amps). The delay in the onset of formation of gas occurs because of the total solubility of CO_2 in the fuel solution.

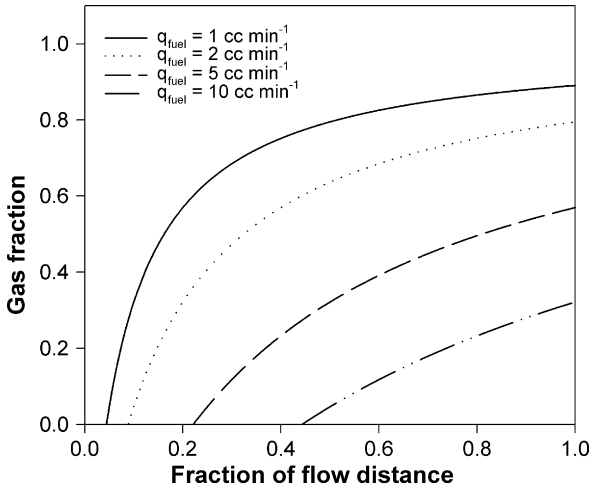

Fig. 2. The void fraction predicted by Eq. (10) is displayed for a range of fuel flow rates with respect to the fraction of the flow distance (T = 60 °C, P = 1 atm, i = 3 Amps). Increasing the liquid flow rate is one way to reduce bubble formation.

2.3. Delaying onset of CO_2 gas formation

The idea of the solution having a maximum carrying capacity for liquid-phase CO_2 can be extended to include additional parameters having the potential for user manipulation. Despite possible detrimental effects on the methanol oxidation reaction, which occurs under acidic conditions, alkaline solutions are suitable for illustration of how gas production might be reduced. In the case of the addition of a hydroxide salt, Eqs. (11) and (12) describe the additional chemical reactions [8]:

$$CO_2 + OH^- = HCO_3^-, \quad (11)$$

$$CO_3^{2-} + H_2O = HCO_3^- + OH^-, \quad (12)$$

where the equilibrium constants are $K_{11} = 6.1 \times 10^7\ l\,mol^{-1}$ and $K_{12} = 1.7 \times 10^{-4}\ mol\,l^{-1}$. At low concentrations an equilibrium is established between CO_3^{2-} and HCO_3^- obeying

$$\frac{[HCO_3^-]}{[CO_3^{2-}]} = \frac{1.7 \times 10^{-4}}{[OH^-]}. \quad (13)$$

Under conditions where OH^- is completely consumed, HCO_3^- is the only species present, Eq. (13) is the only relevant reaction and OH^- acts to solubilize CO_2 on a 1:1 mol basis. In this case, the concentration of OH^- can be inserted into Eq. (7) to form

$$x_{sat} = \frac{6Fq_{feed}(C^{sat}_{CO_2} + C_{OH^-})}{i_x}, \quad (14)$$

where C_{OH} is the molar concentration of hydroxide in the fuel solution. Here, the hydroxide concentration acts as an additional

sink into which CO_2 can exist in the liquid phase. Eq. (9) then becomes

$$q_{CO_2} = \begin{cases} 0 & x \leq \dfrac{6Fq_{\text{fuel}}(C^{\text{sat}}_{CO_2}(T) + C_{OH^-})}{i_x} \\ \dfrac{RT}{P}\dfrac{i_x}{6F}(x - x_{\text{sat}}) & x > \dfrac{6Fq_{\text{fuel}}(C^{\text{sat}}_{CO_2}(T) + C_{OH^-})}{i_x} \end{cases} . \quad (15)$$

Additional terms can be added to Eq. (7) or (14) in a similar fashion, as new methods for retention of CO_2 in the liquid phase become available.

3. Experimental

3.1. Experimental setup

The fuel cell hardware assembly used for the experiments is a 5 cm^2 model provided by Fuel Cell Technologies, Inc. The cell consisted of a pair of POCO graphite blocks with a precision machined single serpentine flow-pattern and gold plated connectors fastened with aluminum end plates. Characteristics of the flow channel included a cross-sectional area of 1 mm^2, an overall centerline length of 325 mm, an open ratio of 65.0%, and fourteen 180° turns with a diameter of 1 mm.

Characteristics for membrane electrode assemblies used in all experiments included an active area of 5 cm^2, an anode catalyst loading of 4.0 mg Pt–Ru cm^{-2}, a cathode catalyst loading of 2.0 mg Pt cm^{-2}, and Nafion-117 polymer electrolyte membrane. The gas diffusion layers at the anode and cathode were carbon cloth and ETEK ELAT®, respectively.

All experiments in this study used the setup shown in Fig. 3. Methanol solution isolated from atmosphere by a nitrogen pad was provided by a computer controlled GA series Micropump™ with steady flow rates available from 0.01 to 50 cm^3 min^{-1}. The standard for all anode fuel solutions was HPLC grade methanol and deionized water (18 MΩ). The methanol concentration for all experiments was 1 mol l^{-1}.

Controlled extra dry oxygen without humidification was provided to the cathode by a feed system consisting of an MKS™ mass flow controller with flow rates available up to 500 scc min^{-1}. A purge gas consisting of ultra pure nitrogen was used to remove oxidant from the system prior to experiments.

Gaseous CO_2 was separated and captured from unreacted methanol solution as it drained from the cell. Oxidant exiting the cathode was vented to atmosphere.

Electrical conditions of the test cell were maintained by a Scribner 890CL fuel cell test load system controlled by a PC running Scribner's proprietary FuelCell® (Version 3.4d). All tests reported here were performed using a cathode feed rate of 100 scc min^{-1}, the cell in a vertical orientation, a current discharge control mode, and atmospheric pressure (101.325 kPa).

3.2. Model verification procedure

Quantification of the rate of CO_2 gas generation for model verification was accomplished through the use of a gas capture device. CO_2 gas separated from the unspent fuel exiting the anode was passed into a chamber isolated from atmosphere. Separating the chamber from atmosphere was a pad of water presaturated with CO_2 to prevent additional unintended absorption of CO_2 gas. The rate of gas generation was then determined by measuring the volume displacement of water with respect to time. Data were taken in sets at various current discharge rates while keeping the operating temperatures, pressures, and fuel flow rates constant.

For verification of the model extension, where hydroxide salts were added to the standard anode fuel solution, the cell was operated with a standard anode fuel solution until it stabilized,

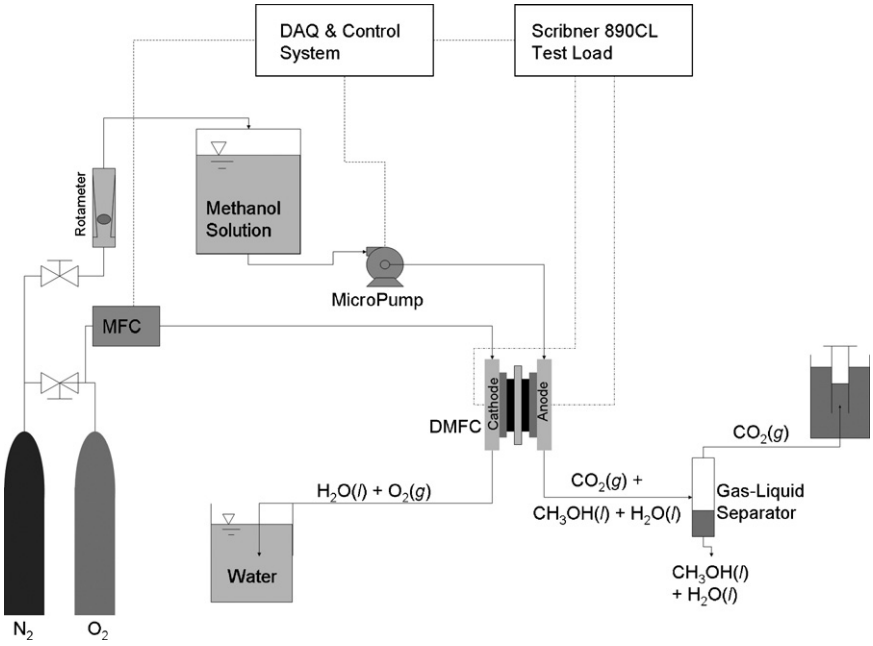

Fig. 3. Schematic of the DMFC test loop and CO_2 gas capture system.

whereupon the source was switched to modified fuel and the above procedure followed. New membrane electrode assemblies were used for both LiOH and KOH experiments.

3.3. Stability experiments with hydroxide salt and amine solutions

Knowing that the addition of an alkaline compound might interfere with the methanol oxidation reaction and that it might adversely affect the Nafion® membrane, experiments were conducted to determine the stability of the membrane electrode assemblies under conditions where hydroxide salts were present after model verification experiments showed promising results. NaOH, LiOH, $Ca(OH)_2$, and ammonium hydroxide were each tested in separate experiments using fresh membrane electrode assemblies. Each test was a total of 65 min long and was conducted at a temperature of 60 °C, an anode flow rate of 5 $cm^3\ min^{-1}$, and at a current discharge rate of 400 mA cm^{-2} (2 Amps). Each test began with standard fuel solution, current was stepped to 400 mA cm^{-2} from open circuit, 5 min was allowed to pass for equilibrium to occur, and fuel was switched to a solution that included an addition of hydroxide salt that resulted in a salt concentration of 0.005 M. After the fuel switch, the electrical performance of the cell was monitored for 60 min.

4. Results and discussion

Eq. (9) predicts a stepwise function where the rate of gas formation increases at a rate proportional to current, but is not present until some onset current where the formation of CO_2 exceeds the carrying capacity of the fuel solution. The carrying capacity of the fuel solution is the maximum rate at which the fuel solution can absorb CO_2, which is a function of the fuel flow rate and the solubility of CO_2 in the solution, which itself is a strong function of both temperature and pressure. While applying the ideal gas law to Eq. (4) alone would predict an increase in gas formation for a temperature rise of 10 °C due to Charles' law, it would not consider the effect of flow rate. Despite a competing effect of temperature on solubility, the flow rate of the fuel solution, if appropriately raised, can compensate for the increase in temperature and actually decrease the rate of gas formation. Fig. 4 compares the results of model verification experiments with predictions of both Eq. (9) and the ideal gas law applied to Eq. (4) while simultaneously demonstrating the shift produced by the delayed onset of gas formation and the overwhelming effect of fuel flow rate. In practice, small bubbles are occasionally witnessed earlier in the flow field than the model predicts (Yang et al.). This is a result of localized CO_2 saturation within the gas diffusion layer.

Yang et al. states that an increase in the sweeping rate of bubbles due to an increase in flow rate causes a reduction in the number of bubbles in the flow field. This can be misinterpreted to mean that that an increase in flow rate causes a reduction in the volume consumed by gas, which Fig. 4 rejects. An assumption of steady state requires that the quantity of CO_2 exiting the cell must equal what is generated, which is dependant solely on the cell's current discharge rate. Without consideration for the CO_2 solubility of the fuel solution, this entire quantity of CO_2 must immediately evolve as gas, which, using the ideal gas equation as the sole correction factor, would produce a greater volume of gas to form regardless of the flow rate and contrary to the data.

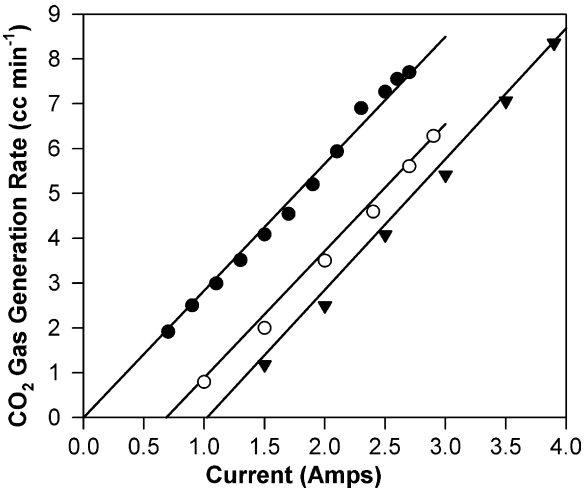

Fig. 4. The delay of gas formation due to CO_2 solubility is illustrated by plotting the rate of CO_2 generation as a function of total current (●: $T = 60$ °C, $Q = 5\ cm^3\ min^{-1}$, pre-saturated fuel solution; ○: $T = 60$ °C, $Q = 5\ cm^3\ min^{-1}$; ▼: $T = 70$ °C, $Q = 10\ cm^3\ min^{-1}$; (- - -) Eq. (5) prediction; (—) Eq. (9) model predictions).

Adjustments to temperature and flow rate may be prohibited by external requirements of the cell, or they may not be sufficient to completely eliminate gas under high current discharge conditions. Additionally, changes to flow rate and temperature may cause more problems due to pumping requirements and methanol crossover than they solve by the reduction of two-phase flow, thus is is of interest to enhance the solubility of CO_2 in the fuel system.

Eq. (15) predicts that additional control over the effective solubility of CO_2 in the fuel solution can be achieved by the addition of components that react with CO_2. Of particular interest are reactions involving hydroxides and amines, both well understood and used in industrial CO_2 stripping operations. Potassium hydroxide, tested in a concentration of 0.0053 M (Fig. 5), causes a shift in the rate of gas formation that matches the prediction of Eq. (15). It is worth pointing out that the addition of KOH in a concentration of 0.0053 M produces a nearly identical shift to that of increasing the flow rate in Fig. 4. Similar reduction occurs with LiOH, which is again predicted by Eq. (15). Increasing the concentration to 0.01 M, the rate of gas production continues to decrease, and along with it, the onset of gas formation is delayed further (Fig. 6).

Despite significant reduction in CO_2 formation and model verification, when hydroxide was added the cell did not remain stable. Experiments were conducted to investigate the stability of membrane electrode assemblies due to the previous observations and to explore other reaction possibilities. After an initial drop in power density at 2 Amps, the cell using ammonium hydroxide experienced a linear decay of 0.45 mW $cm^{-2}\ min^{-1}$ over the final 35 min of the experiment, resulting in an overall 34% drop in power density. Sodium hydroxide has a similar rate of decay

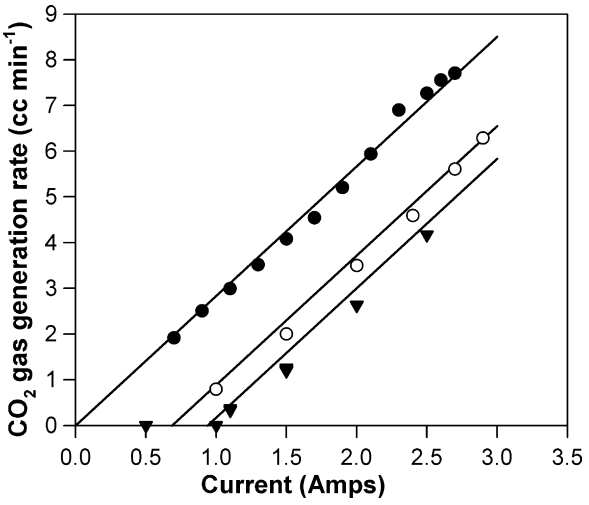

Fig. 5. The delay of gas formation when KOH is added to the fuel solution is illustrated by comparing the rate of CO_2 gas generation as a function of current (●: $T = 60\,^{\circ}C$, $Q = 5\,cm^3\,min^{-1}$, pre-saturated fuel solution; ○: $T = 60\,^{\circ}C$, $Q = 5\,cm^3\,min^{-1}$; ▼: $T = 60\,^{\circ}C$, $Q = 5\,cm^3\,min^{-1}$, 0.0053 M KOH; (- - -) Eq. (5) prediction; (—) Eq. (15) predictions).

at $0.37\,mW\,cm^{-2}\,min^{-1}$ over the final 35 min, however it experiences a larger initial drop, resulting in a 33% overall drop in power density for the experiment. Lithium hydroxide fares much better with a decay rate nearly half that experienced by ammonium hydroxide at $0.23\,mW\,cm^{-2}\,min^{-1}$ which, with inclusion of the initial drop, results in a 23% decrease in power density. Calcium hydroxide, exhibits somewhat different behavior: there is an initial rise in current density, followed by a steep decline with instabilities growing in magnitude. Fig. 7 compares the results of these studies. Interactions of the hydroxide salt cations with the Nafion® membrane, which has proton conducting sites that can potentially undergo permanent replaced by +1 cations, is the likely explanation for the reduction in power output.

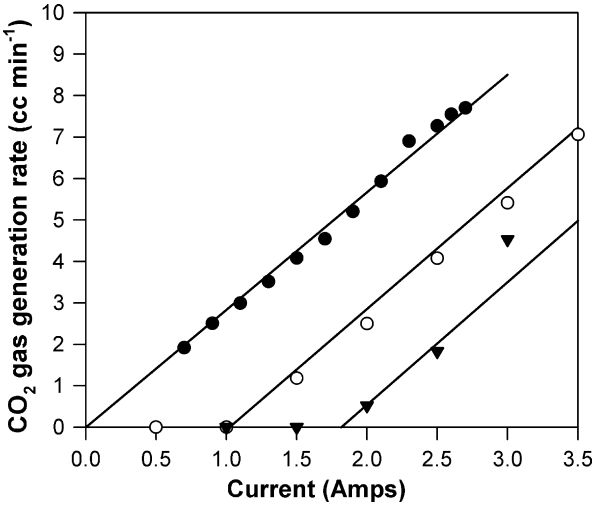

Fig. 6. The delay of gas formation when LiOH is added to the fuel solution is illustrated by comparing the rate of CO_2 gas generation as a function of current (●: $T = 60\,^{\circ}C$, $Q = 5\,cm^3\,min^{-1}$, pre-saturated fuel solution; ○: $T = 70\,^{\circ}C$, $Q = 10\,cm^3\,min^{-1}$; ▼: $T = 70\,^{\circ}C$, $Q = 10\,cm^3\,min^{-1}$, 0.01 M LiOH; (- - -) Eq. (5) prediction; (—) Eq. (15) predictions).

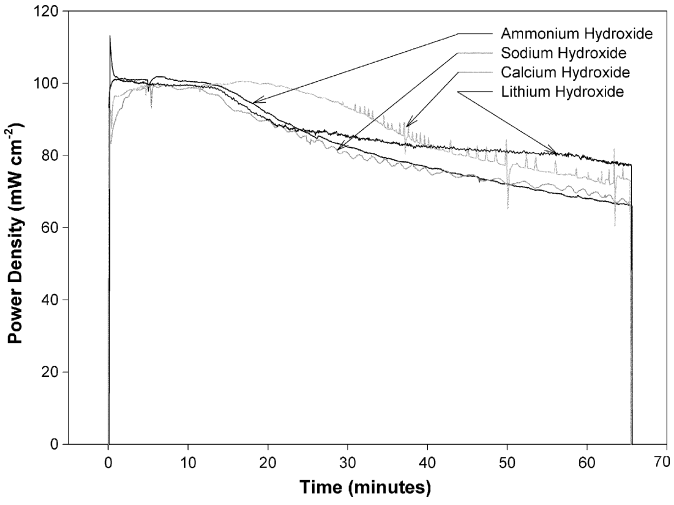

Fig. 7. The power density for cells operated with selected hydroxide salts is plotted against time for identical operating conditions of $T = 60\,^{\circ}C$, $Q = 5\,cm^3\,min^{-1}$, $i = 2$ Amps, and $[OH^-] = 0.005$ M.

Compelling visual evidence in Fig. 7 indicates that the results of the calcium hydroxide experiment differed from sodium, ammonia, and lithium counterparts. The calcium cation was not expected to cause the same permanent replacement of proton sites in the Nafion® membrane due to the +2 state of the calcium ions. The result of the reaction is insoluble calcium carbonate, which immediately precipitates out of solution eventually blocking the flow field and any other part of the fuel path downstream of the cell. The rapid rate of reaction and, consequently, the rapid rate of solid formation, prevent effective downstream filtering and are the cause of the instabilities visible in Fig. 7.

5. Conclusions

A model that explains the rate of CO_2 gas formation at the anode of a DMFC including a function of the cell's output current, operating temperature, operating pressure, fuel flow rate, and the solubility of CO_2 in the fuel solution, which is also a strong function of temperature is presented and verified. The onset delay of gas formation is a function of solubility, which may be exploited by DMFC designers to reduce or possibly eliminate the formation of gas by properly tuning the operating parameters of the cell. Additionally, the expression developed to describe the rate of gas formation can be extended to include additional parameters capable of manipulation for design purposes.

For the first time, the solubility of CO_2 in DMFC fuel is increased by addition of OH^-. The results, again in agreement with the model, show that CO_2 gas can be reduced or potentially eliminated through the addition of components to the fuel system.

Long-term durability of the membrane electrode assembly was used as screening criterion in an exploration of possible candidates for extending the delay of gaseous CO_2 onset. While hydroxide salts were promising candidates due to their performance in model validation experiments, declines in power output of over 20% in an hour are unacceptable for any benefit received.

Encapsulating the ions potentially harmful to the MEA in such a way such that reactions are still allowed to take place, possibly with liquid membrane emulsions, might be a good avenue of future study.

Acknowledgement

This work was supported by the United States Army under Agreement no. DAAB07-03-3-K414.

References

[1] J. Han, J. Ge, H. Liu, J. Power Sources 164 (2007) 90–93.
[2] Y.H. Cai, J. Hu, H.P. Ma, B.L. Yi, H.M. Zhang, Electrochim. Acta 51 (28) (2006) 6361–6366.
[3] M.M. Mench, S. Boslet, S. Thynell, J. Scott, C.Y. Wang, Proceedings of the Symposium on Direct Methanol Fuel Cells, The 199th Electrochem. Soc. Proc. Series, Princeton, NJ, 2001.
[4] Argyropoulos, K. Scott, W.M. Taama, J. Appl. Electrochem. 31 (2001) 823–832.
[5] H. Yang, T.S. Zhao, Q. Ye, J. Power Sources 139 (2005) 79–90.
[6] J. Xia, M. Jodecke, A. Kamps, G. Maurer, J. Chem. Eng. Data 49 (2004) 1756–1759.
[7] J.J. Carroll, J. Slupsky, A. Mather, J. Phys. Chem. Ref. Data 20 (6) (1991) 1201–1209.
[8] G. Astarita, Mass Transfer with Chemical Reaction, Elsevier Publishing Company, Amsterdam, 1967.